THE JOURNAL OF BIOLOGICAL CHEMISTRY VOL. 289, NO. 23, pp. 16349–16361, June 6, 2014
Published in the U.S.A.

Allosteric Inhibitors of the Eya2 Phosphatase Are Selective and Inhibit Eya2-mediated Cell Migration*

Received for publication, March 21, 2014, and in revised form, April 17, 2014 Published, JBC Papers in Press, April 22, 2014, DOI 10.1074/jbc.M114.566729

Aaron B. Krueger[‡], David J. Drasin[§], Wendy A. Lea[¶], Aaron N. Patrick[§], Samarjit Patnaik[¶], Donald S. Backos[‖], Christopher J. Matheson[‖], Xin Hu[¶], Elena Barnaeva[¶], Michael J. Holliday[‡], Melanie A. Blevins[‡], Tyler P. Robin[§], Elan Z. Eisenmesser[‡], Marc Ferrer[¶], Anton Simeonov[¶], Noel Southall[¶], Philip Reigan[‖], Juan Marugan[¶1], Heide L. Ford[§2], and Rui Zhao[‡3]

From the [‡]Department of Biochemistry and Molecular Genetics, University of Colorado School of Medicine, Aurora, Colorado 80045, the [§]Department of Pharmacology, University of Colorado School of Medicine, Aurora, Colorado 80045, the [¶]National Center for Advancing Translational Sciences, National Institutes of Health, Bethesda, Maryland 20892, and the [‖]Department of Pharmaceutical Sciences, Skaggs School of Pharmacy and Pharmaceutical Sciences, University of Colorado School of Pharmacy, Aurora, Colorado 80045

Background: The phosphatase activity of Eya is important for transformation, invasion, migration, and metastasis of breast cancer cells.
Results: A class of *N*-arylidenebenzohydrazide compounds specifically inhibits the phosphatase activity of Eya2 but not Eya3.
Conclusion: This class of compounds likely acts through an allosteric mechanism.
Significance: These inhibitors may be developed into chemical probes or anti-cancer drugs.

Eya proteins are essential co-activators of the Six family of transcription factors and contain a unique tyrosine phosphatase domain belonging to the haloacid dehalogenase family of phosphatases. The phosphatase activity of Eya is important for the transcription of a subset of Six1-target genes, and also directs cells to the repair rather than apoptosis pathway upon DNA damage. Furthermore, Eya phosphatase activity has been shown to mediate transformation, invasion, migration, and metastasis of breast cancer cells, making it a potential new drug target for breast cancer. We have previously identified a class of *N*-arylidenebenzohydrazide compounds that specifically inhibit the Eya2 phosphatase. Herein, we demonstrate that these compounds are reversible inhibitors that selectively inhibit the phosphatase activity of Eya2, but not Eya3. Our mutagenesis results suggest that this class of compounds does not bind to the active site and the binding does not require the coordination with Mg^{2+}. Moreover, these compounds likely bind within a site on the opposite face of the active site, and function as allosteric inhibitors. We also demonstrate that this class of compounds inhibits Eya2 phosphatase-mediated cell migration, setting the foundation for these molecules to be developed into chemical probes for understanding the specific function of the Eya2 phosphatase and to serve as a prototype for the development of Eya2 phosphatase specific anti-cancer drugs.

The Eya 1–4 (eyes absent family of proteins) were first discovered as essential coactivators (1–4) of the homeobox transcription factor Six1 (2, 5–11). Both Six1 and Eya proteins are necessary for cellular proliferation in a number of different cell types (2, 8, 12). In support of a cooperative interaction between Six1 and Eya, the Eya1 knock-out (KO) mouse phenocopies the Six1 KO mouse, and organ defects in both KO mice are due to a decrease in proliferation and an increase in apoptosis (13, 14). Both Six1 and Eya1 are linked to branchio-oto-renal syndrome, which is characterized by branchial defects, hearing loss, and renal abnormalities (9, 10). These data suggest that Six1 and Eya cooperate in normal development of human and mouse tissues. Importantly, the Six1-Eya complex is overexpressed in many different tumor types, including Wilms' tumor, ovarian cancer, acute leukemia, malignant peripheral nerve-sheath tumors, glioblastomas, and breast cancer (8, 15–20). We have recently demonstrated that Eya2 knockdown inhibits the ability of Six1 to induce TGF-β signaling, epithelial-to-mesenchymal transition, and tumor-initiating cell characteristics in breast cancer, properties that are associated with Six1-induced breast tumorigenesis and metastasis (17). We further demonstrated that a direct interaction between Six1 and Eya2 is required for epithelial-to-mesenchymal transition and metastasis (21). Furthermore, analyses of microarray data from 295 breast tumors demonstrated that coordinated overexpression of Six1 and Eya together significantly predict decreased time to relapse and metastasis as well as shortened survival, whereas the overexpression of individual genes does not (17). These clinical data strongly suggest that the Six1-Eya complex mediates breast tumorigenesis, and confers poor prognosis in breast cancer.

* This work was supported by the Molecular Libraries Initiative of the National Institutes of Health Roadmap for Medical Research, National Institutes of Health Grant R03DA030559 (to R. Z. and H. L. F.). This work was also supported by Department of Defense Synergistic Idea Award BC084105 (to H. L. F. and R. Z.), an American Association for Cancer Research and Breast Cancer Research Foundation grant (to H. L. F. and R. Z.), a State of Colorado Proof of Concept grant (to R. Z. and H. L. F.), National Institutes of Health Small Business Technology Transfer Grant R41CA180347 (to H. L. F. and R. Z.), and a Cancer League of Colorado grant (to P. R., H. L. F., and R. Z.).
[1] To whom correspondence may be addressed. Tel.: 301-217-9198; Fax: 301-217-5736; E-mail: maruganj@mail.nih.gov.
[2] To whom correspondence may be addressed. Tel.: 303-724-3509; Fax: 303-724-3663; E-mail: heide.ford@ucdenver.edu.
[3] To whom correspondence may be addressed. Tel.: 303-724-3269; Fax: 303-724-3215; E-mail: rui.zhao@ucdenver.edu.

Eya proteins also contain a unique protein tyrosine phosphatase activity in their highly conserved Eya domain (ED).[4] This phosphatase activity has been demonstrated to switch the Six1 transcriptional complex from a repressor to an activator for some Six1-induced genes (2). In *Drosophila*, although the phosphatase activity of Eya is not globally required for the ability of Six1 to induce transcription, it is required to induce transcription of a subset of genes (1). The Eya proteins therefore represent the first transcriptional co-activators with intrinsic phosphatase activity to modulate transcription (2, 3, 22). Eya proteins are the founding members of a class of non-thiol-based protein phosphatases belonging to the haloacid dehalogenase (HAD) family of enzymes. The HAD family of phosphatases use an aspartic acid (Asp) as the catalytic active-site residue instead of the more commonly used cysteine (Cys) used by most cellular phosphatases (23). Some HAD members, such as Scp1 and chronophin, dephosphorylate protein substrates, whereas substrates of many HAD phosphatases are small molecules (3, 23). All other known HAD protein phosphatases are Ser/Thr phosphatases, leaving Eya as the sole member targeting phosphorylated Tyr (23, 24). Structurally, HAD members share a highly conserved catalytic core but contain a variable cap structure. Eya members have a unique helical bundle as the cap that is not observed in any other HAD protein (23, 25).

Recently, the tyrosine phosphatase activity of Eya has been shown to be critical for transformation, migration, invasion, and metastasis of breast cancer cells (26). Although it has been argued that the phosphatase activity of Eya is not essential for its ability to induce proliferation (26), Pestell and colleagues (27) recently demonstrated that the Eya1 phosphatase activity is in fact necessary for Eya-induced proliferation of breast cancer cells. In addition, the phosphatase activity of Eya plays a role in the DNA damage response via its ability to dephosphorylate histone variant H2AX upon DNA damage, leading cells to the repair instead of apoptosis pathway (24, 28). These data suggest that inhibiting Eya phosphatases may not only inhibit tumor onset and progression but may also sensitize cells to commonly used chemotherapeutics that act through inducing DNA damage. Importantly, drugs that target the Eya phosphatases may confer limited side effects as most Eya family members are highly expressed in developing tissues but are not expressed in most normal adult tissues (29).

We have previously identified a series of structurally related small molecule compounds that specifically inhibit the Eya2 phosphatase using high throughput screening (HTS) (30). In this work, we describe characterization of the mechanism of action of these inhibitors, which suggests that this class of compounds functions as allosteric inhibitors of the Eya2 phosphatase activity. We also demonstrate that this class of compounds inhibits Eya2-mediated migration of breast cells. These studies set the foundation for further developing these inhibitors into chemical probes or potential therapeutic agents targeting the Eya phosphatase.

[4] The abbreviations used are: ED, Eya domain; HAD, haloacid dehalogenase(s); HTS, high throughput screening; OMFP, 3-*O*-methylfluorescein phosphate; ITC, isothermal calorimetry; HBM, helix-bundle-motif; DMSO, dimethyl sulfoxide; FDP, fluorescein diphosphate; HSQC, heteronuclear single quantum coherence.

EXPERIMENTAL PROCEDURES

Protein Expression and Purification—Eya2 ED (residues 253–538) was subcloned into a pGEX-6p1 vector (GE Healthcare) and the protein was expressed as a GST-fusion protein in *Escherichia coli*. The protein was first purified on a glutathione column. GST was then cleaved off using PreScission protease and eluted Eya2 ED was further purified on a Superdex 200 (S200) column (GE Healthcare).

Eya Phosphatase Assays—Eya activity was measured in 50-μl reactions using black, 96-well, half-volume microtiter plates (Greiner Bio-one) with the substrate OMFP (3-*O*-methylfluorescein phosphate, Sigma-Aldrich), which is converted to a fluorescent product OMF upon dephosphorylation. The assay conditions used were 50 mM MES, pH 6.5, 50 mM NaCl, 1.25 mM $MgCl_2$, 0.05% BSA, and 1 mM DTT, and the reaction contained 50 nM Eya2 ED and 100 μM OMFP. Reactions were started by the addition of OMFP, preceded for 1 h at room temperature followed by terminating the reaction with the addition of 75 mM EDTA. Fluorescence intensity was measured at 485/515 nm excitation/emission on a Fluoromax-3 plate reader (Horiba Jobin Yvon).

Isothermal Titration Calorimetry—Eya proteins were purified via S200 in isothermal titration calorimetry (ITC) buffer (50 mM $NaPO_4$ buffer, pH 6.5, 50 mM NaCl). Inhibitor solutions were prepared by diluting from a DMSO stock into ITC buffer. DMSO was added to the protein solution to the same concentration as the inhibitor solution (0.2%), and all solutions were degassed. ITC experiments were performed with a VP-ITC microcalorimeter (MicroCal, Inc., GE Healthcare) at 25 °C. Due to low solubility of inhibitors in aqueous buffer, we injected Eya protein into the sample cell containing inhibitor, and the reference cell was filled with ITC buffer. After a 2-μl initial injection, 10-μl aliquots of 250 μM protein was added stepwise at 5-min intervals into the sample cell containing 20 μM inhibitor until saturation. Origin (version 7.0) was used to analyze data with embedded calorimetric fitting programs to generate the binding curves.

Enzymatic Kinetics—All kinetic experiments were performed using 384-well black medium binding plates (Greiner Bio-One). Fluorescein diphosphate (FDP, Anaspec) was prepared as a 100 mM stock solution in Eya2 ED assay buffer (25 mM HEPES, 50 mM NaCl, 5 mM $MgCl_2$, pH 6.5) and stored in single-use aliquots at −80 °C and protected from light. Both Eya2 ED and FDP stock solutions in assay buffer were diluted to working solutions in Eya2 ED buffer with freshly added 5 mM DTT and 0.33% BSA prior to the assay. To calculate K_m values and generate a Lineweaver-Burke plot for Eya2 ED phosphatase activity with FDP as substrate, we performed kinetic measurements at various concentrations of FDP and compound. Briefly, 50 nl of compound (NCGC00249327) at 10, 3.3, 1.1, 0.37, 0.12, 0.04, 0.014, or 0 mM in DMSO were added by ATS Acoustic Liquid Dispenser (EDC Biosystems) to empty wells of a plate. Immediately after, 5 μl of 0.5 μM Eya2 ED were added and the solutions incubated for 10 min at room temperature. Next, 5 μl of FDP substrate solutions at 8, 4, 2, 1, 0.5, 0.25, 0.125, or 0.063 mM were added to the wells using a CyBi®-well 384-channel simultaneous pipettor (CyBio, U.S., Inc.). The plate was briefly

spun down, and fluorescence intensity was measured every 5 min for a 1-h time course using a ViewLux Imager (Perkin Elmer, Inc.) with the following settings: excitation wavelength of 485 nm, emission wavelength of 525 nm, energy light of 750, and exposure time of 0.5 s. Kinetic analysis was performed using GraphPad Prism (version 4, GraphPad Software).

Reversibility Assay—The enzyme at a concentration that is 100-fold (100 nM) more than what is required for the activity assay (1 nM) is incubated with a concentration of inhibitor (40 μM) equivalent to 10-fold of the IC_{50}. The enzyme-inhibitor complex is then diluted 100-fold and substrate is added to initiate the enzymatic reaction. The enzymatic activity at different time points (1–3 h) is compared with that of a similar sample of enzyme incubated and diluted in the absence of inhibitor. If the inhibition is reversible, the enzyme activity will recover to roughly the uninhibited level (the inhibition could be slowly reversible where the enzyme will take longer to reach full activity after dilution). If the inhibition is irreversible, the enzymatic activity will remain very low after dilution because the compounds have irreversibly inactivated the enzyme.

Cell Lines—Stable integration of full-length human Eya2 or phosphatase-dead Eya2 (D274N) in MCF10A cells was achieved through retroviral transduction. Eya2 or D274N was cloned into pMSCV-IRES-YFP backbone, and BOSC cells were used to package viral particles. YFP-positive cells were sorted 1 week after infection.

Motility Assay—Motility was measured using a gap closure assay, where a silicone μ-well insert (Ibidi, Verona, WI) in a 24-well plate was used to create an ~500-μm gap between 40,000 cells/chamber that were plated overnight. Photos were taken of the gap immediately after removing the insert and adding 10 μM compound (or vehicle control) containing medium and then again 6 h later on a CKX41 microscope (Olympus, Tokyo, Japan). Distance migrated was determined by subtracting the size of the gap at the end time point from the size of the gap at the initial time point, using DP2-BSW software (version 2.2; Olympus). Statistics were calculated with Prism (version 5.0, GraphPad, San Diego, CA).

Thermal Shift Experiments—To provide evidence for the binding between hydrazides and Eya2 ED, thermal shift experiments were performed to evaluate whether Eya2 ED melting temperature (T_m) could be shifted in the presence of different concentrations of hydrazides. Compounds were serially diluted in DMSO in 96-well polypropylene plates (Thermo Fisher Scientific). A mixture of 49 μl of Eya2 ED and SYPRO Orange (5000× stock solution, Invitrogen) were transferred to a 96-well skirted thin-wall PCR plate (Bio-Rad) with a final concentration of 1 μM and 5×, respectively. Compounds prepared in the aforementioned mother plate were subsequently added to the protein-dye mixture, with final concentrations ranging from 0.34 nM to 200 μM (final volume, 50 μl). DMSO alone was also transferred within each compound dilution series as a control sample. DMSO concentration was consistent across each dilution series and was maintained at 2%. The plate was sealed with Optical-Quality Sealing Tape (Bio-Rad) and was centrifuged at 1000 rpm for 20 s before heating commenced. Plate heating was performed on an iQ5 real-time PCR detection system (Bio-Rad) from 20 to 95 °C with an increment of 1 °C and a ramping rate of 0.1 °C/s. A CCD camera was used to measure SYPRO Orange fluorescence through a filter set corresponding to excitation and emission wavelengths of 490 and 575 nm, respectively. Protein melting temperature was obtained from an EXCEL-based worksheet (provided by Structure Genomics Consortium) and GraphPad Prism (version 4).

NMR Spectroscopy—^{15}N-labeled Eya2 ED was expressed in *E. coli* in the presence of $^{15}NH_4Cl$ in minimal medium and purified similarly as the unlabeled Eya2 ED. Optimal NMR buffer conditions were determined to be 50 mM Bicine, pH 7.5, 50 mM NaCl, 0.5% glycerol. Maximum Eya2 ED concentration used was 150 μM due to aggregation at higher concentrations. HSQC experiments were collected at 25 °C on a Varian 900 MHz at a concentration of 150 μM Eya2 ED. Compound was added to saturate Eya2 ED while keeping DMSO concentration below 0.1% DMSO.

UV-visible Spectra Analysis of Selected Hydrazides—Compounds were dissolved in acetonitrile at a final concentration of 25 μM with final Mg^{2+} concentration at 0, 0.5, 1, 5, 10, 25, 50, 100, and 200 mM. UV-visible spectra were obtained using an Agilent 8453 UV-visible Spectrophotometer (Agilent Technologies) in 0.1-cm quartz cuvette at room temperature.

Molecular Docking—The AutoDock program (version 4.0) was used to dock the compounds to the active site of the crystal structure of Eya2 ED (Protein Data Bank code 3HB1). The active site of the protein was defined by a grid of 70 × 70 × 70 points with a grid spacing of 0.375 Å centered at the Mg^{2+} ion. The Lamarckian genetic algorithm was applied with 100 runs, and the maximum number of energy evaluations was set to 2×10^6. Results differing by less than 1.5 Å in positional root mean square deviation of substrate were clustered, and the final binding conformations were represented by the one with the most favorable free energy of binding. The optimal binding complexes were subjected to a stepwise energy minimization and molecular dynamics simulations.

Docking at the allosteric site was performed with the flexible docking protocol (31) of Accelrys Discovery Studio (version 3.1, Accelrys Software) using the crystal structure of Eya2 ED (Protein Data Bank code 3GEB). Predicted binding-induced changes in protein structure were determined by the conjugate gradient minimization protocol using a CHARMM force field and the Generalized Born implicit solvent model (32). All minimizations converged to a root mean square gradient of <0.001 kcal/mol.

RESULTS

HTS Identified a New Chemical Series That Specifically Inhibits the Phosphatase Activity of Eya2—We have identified a series of structurally related compounds containing an *N*-arylidenebenzohydrazide core that inhibits the phosphatase activity of Eya2 with varying potency using an OMFP-based phosphatase assay and the Eya2 ED (structures of selected members of this class are shown in Fig. 1*A*) (30). Initial enzyme kinetics studies indicated that MLS000544460 exhibits a mixed mode behavior between competitive and non-competitive inhibition (30). Additional kinetic studies indicate that the competitive nature of these molecules depended on the concentration

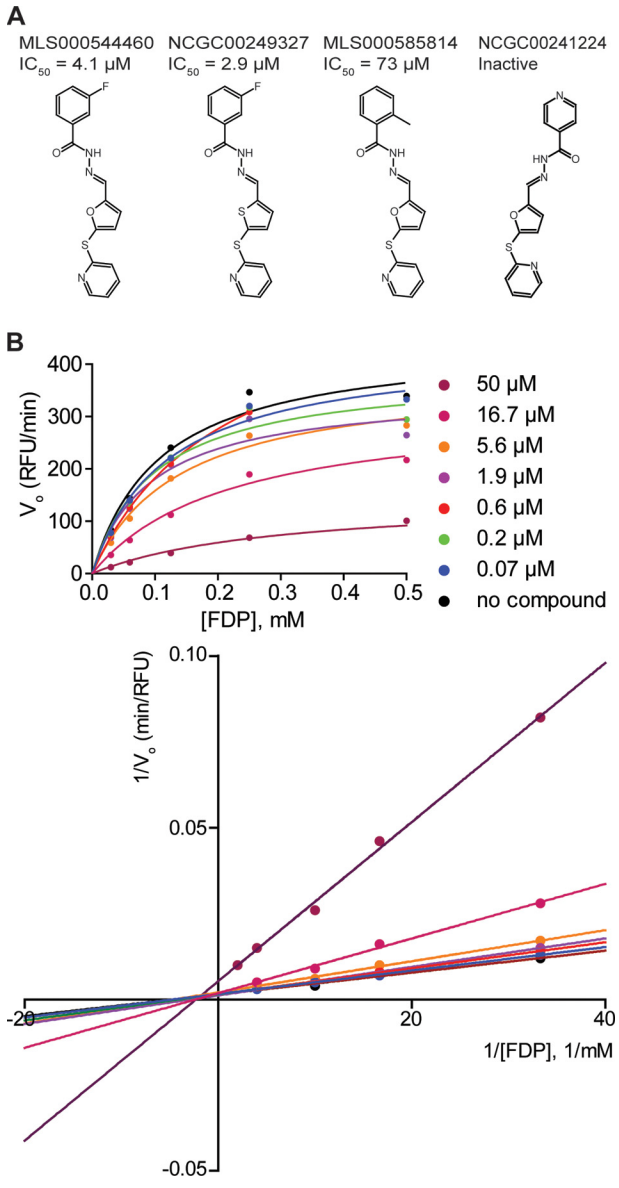

FIGURE 1. **Eya2 ED enzyme kinetic experiments indicate that the *N*-arylidenebenzohydrazide-containing compounds are non-competitive inhibitors at high Mg^{2+} concentrations (5 mM).** *A*, chemical structures of representative compounds identified directly in HTS (MLS000544460 and MLS000585814), a commercially available compound that has slightly higher potency (NCGC00249327), and a structurally related but inactive compound (NCGC00241224). *B*, saturation curve for Eya2 ED showing initial rate with FDP concentration at each concentration of inhibitor NCGC00249327 (*top*). A Lineweaver-Burk plot shows non-competitive inhibition by NCGC00249327 given that the plots have the same *x* intercept as uninhibited enzyme and differing slopes and *y* intercepts. *RFU,* relative fluorescence units.

of Mg^{2+} in the assay. At a high concentration of Mg^{2+} (5 mM), the compounds display a non-competitive behavior (Fig. 1*B*), whereas at a low concentration (5 μM), they behave in a mixed mode manner (30). All of our enzymatic assays reported in this work were performed at high Mg^{2+} concentrations where the compounds are non-competitive.

We have previously shown that these compounds do not inhibit three other cellular phosphatases (Scp1, PPM1A, and PTP1B), demonstrating specificity toward the Eya2 ED (30). Because there are multiple Eya family members with high homology in the ED, we tested the ability of this series of compounds to inhibit other Eya family members. Using the OMFP-based phosphatase assay, we demonstrated that this class of compounds has no discernible inhibition against the Eya3 ED (we have not been able to express and purify sufficient quantities of human Eya1 or Eya4 ED to test against these other Eya family members) (Fig. 2*A*). To further validate this selectivity, we measured the binding affinity of compound MLS000544460 to Eya2 ED and Eya3 ED using ITC. MLS000544460 binds to the Eya2 ED with a K_D of 2.0 ± 0.3 μM, but it does not bind Eya3 ED, indicating that indeed this class is highly selective toward Eya2 (Fig. 2*B*).

MLS000544460 Inhibits Eya2-mediated Cell Migration—We next generated stable human Eya2, Eya2 phosphatase-dead (D274N), and YFP (as a negative control) expressing MCF10A cells. We analyzed Eya2-dependent motility using a gap closure assay, in which each of the three cell lines were treated with vehicle control (DMSO), an inactive compound NCGC00241224, and the active compound MLS000544460 at 10 μM. We found that Eya2 induces an increase in migration over the YFP control, whereas phosphatase-dead Eya2 does not, indicating that the phosphatase activity of Eya2 is important for the migration of MCF10A cells, consistent with previous reports (33) (Fig. 3, the DMSO columns). Compound MLS000544460 inhibits Eya2-mediated cell migration, whereas the inactive compound NCGC00241224 does not (Fig. 3). The above data indicate that the Eya2 phosphatase is required for cell migration and that this migration can be inhibited by our lead compound targeting the phosphatase activity of Eya2.

MLS000544460 Does Not Require Mg^{2+} for Binding to Eya2 ED—We next explored the mechanism of action of this class of compounds. One possible mechanism of inhibition for these compounds is to serve as Mg^{2+} chelators because these compounds contain a number of heteroatoms that could coordinate a Mg^{2+} ion (Fig. 4*A*). We evaluated UV spectra of compound MLS00054460 in the presence of increasing concentrations of Mg^{2+} to examine this possibility. There is no change in the UV spectra of MLS00054460 in aqueous buffers (including the phosphatase assay buffer) with increasing concentrations of Mg^{2+}, indicating that this compound has very low, if any, affinity to Mg^{2+} in aqueous solution. To evaluate the capacity of these molecules to complex Mg^{2+} in a more lipophilic environment, as a mimetic of the enzymatic active site, we further evaluated the UV spectra of 25 μM MLS000544460 in 100% acetonitrile (34) with increasing concentrations of Mg^{2+}. We observed a dose-dependent shift in the maximum absorbance wavelength (λ_{max}) from 322 (0 mM Mg^{2+}) to 334 nm (100 mM Mg^{2+}) (Fig. 4, *B* and *C*). Similar studies using the monovalent cation Na^+ produced no discernible shift (Fig. 4*D*), indicating that these compounds have intrinsic affinity for Mg^{2+} in a more lipophilic environment similar to acetonitrile but not for other cations such as Na^+. We subsequently examined the UV spectrum of a low activity inhibitor, MLS000585814 (IC_{50} = 73 μM) upon increasing Mg^{2+} concentrations. A similar, dose-dependent shift in λ_{max} was observed from 316 nm (0 mM Mg^{2+}) to 327 nm (50 mM Mg^{2+}) (Fig. 4, *E* and *F*). Although this compound has low activity in the inhibition assay, it retains the ability to bind Mg^{2+} with similar affinity as the more potent

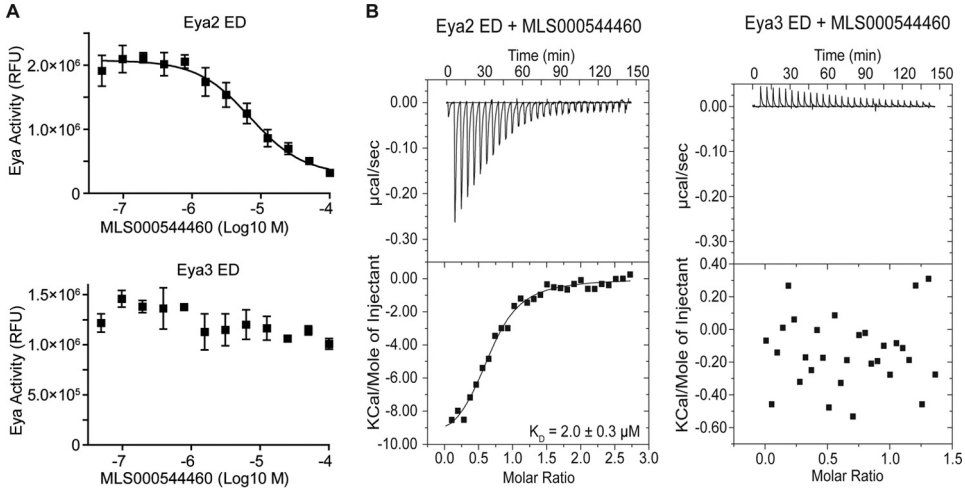

FIGURE 2. **The *N*-arylidenebenzohydrazide-containing compounds selectively inhibits Eya2.** *A*, MLS000544460 inhibits Eya2 but not Eya3 in an OMFP-based phosphatase assay. *B*, MLS000544460 binds to Eya2 ED (K_D, 2.0 ± 0.3 μM) but not Eya3 ED in an ITC experiment. *RFU*, relative fluorescence units.

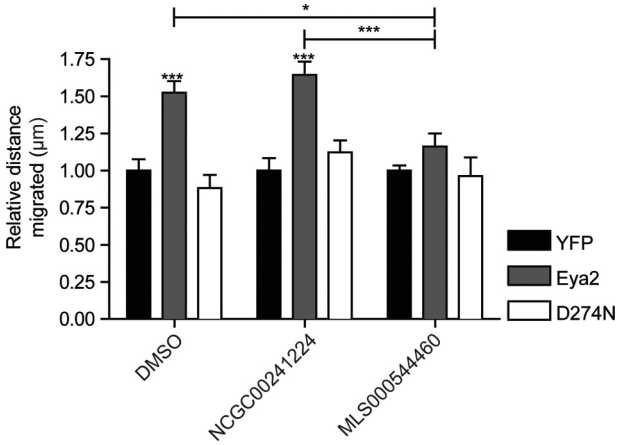

FIGURE 3. **MLS000544460 inhibits Eya2-dependent cell migration.** Compound MLS000544460 (10 μM) inhibits Eya2 phosphatase-dependent migration of MCF10A cells, in a gap closure migration assay for 6 h, whereas the structurally similar but inactive compound NCGC00241224 has no effect. *, $p < 0.05$; ***, $p < 0.001$, two-way analysis of variance.

compound MLS000544460 (Fig. 4, *C* compared with *F*). These data suggest that the binding affinity of this series of compounds to Eya2 ED is the dominating factor for inhibitory activity and not their intrinsic binding affinity to Mg^{2+}.

We also carried out protein thermal shift experiments to examine the binding interaction between this class of compounds and Eya2 ED in the presence or absence of Mg^{2+}. These compounds stabilize Eya2 ED (reflected by an increase of T_m) when exogenous Mg^{2+} is removed by the addition of 5 mM EDTA (Fig. 4*G*), suggesting that the binding between Eya2 ED and these compounds does not require Mg^{2+}. We observed a good correlation between the increase in T_m and the IC_{50} values of the compounds in our series (Fig. 4*G*), indicating that Eya2 binding is the dominant factor for inhibiting the enzyme. Because the increase in T_m values induced by a compound in a chemical series correlates with its affinity toward the protein (35), these data suggest that the compounds with greater affinity toward Eya2 ED have an increased inhibitory capacity (lower IC_{50}).

We next preformed ITC experiments to further examine binding affinities between the inhibitor and Eya2 ED in the presence and absence of Mg^{2+}. We demonstrated that MLS000544460 binds to the Eya2 ED (containing only the Mg^{2+} carried through purification) with a K_D value of 2.0 ± 0.3 μM (Fig. 1*C*). When 5 mM exogenous Mg^{2+} is added, the K_D shifts to 6.1 ± 1.2 μM, implying that Mg^{2+} can potentially interfere with compound binding (Fig. 4*H*). When Eya2 ED is dialyzed into 10 mM EDTA to remove Mg^{2+}, it binds MLS000544460 with a higher affinity (K_D = 0.80 ± 0.04 μM), indicating that this class of compounds does not require Mg^{2+} for its interaction with the Eya2 ED (Fig. 4*I*). Furthermore, we demonstrated that the structurally related but inactive compound NCGC00241224 does not bind to Eya2 ED in ITC experiments, indicating that the binding of this chemical series is driven by specific interactions of chemical moieties in the active compounds rather than nonspecific binding caused by the common chemotype within this class (Fig. 4*J*).

MLS000544460 Is a Reversible Inhibitor—Another possible mechanism of action for these compounds is that the hydrazide functional group provides a reactive chemical moiety that irreversibly binds to the enzyme. To evaluate this possibility, we conducted a traditional irreversibility experiment. (Details of the methods are described under "Experimental Procedures.") We first examined the inhibition capacity of 0.4, 4.0, and 40 μM MLS000544460 after incubation with 1 nM Eya2 ED for 1 h. We observed a clear dose-dependent inhibition with an $IC_{50} \sim 4$ μM. Next, 100 nM Eya2 ED was incubated with 40 μM compound for 10 min. The sample was diluted 100-fold to 1 nM Eya2 ED and incubated for 1 to 3 h (Fig. 5). Substrate was added, and enzyme activity was measured after 20 min. Eya2 ED essentially regains full activity after dilution compared with control (100× (40 μM) *versus* 100× (no compound)), indicating that these inhibitors are reversible. However, the enzyme slowly regains its activity after the dilution and requires ~3 h for almost complete functional recovery (compare the 1- and 3-h incubation panel), indicating a slow dissociation rate and a long occupation time on ED. The reduced activity (~80%) for the 100× (no compound) sample is likely caused by partial precipitation and potential denaturation of the enzyme, observed at high compound concentrations.

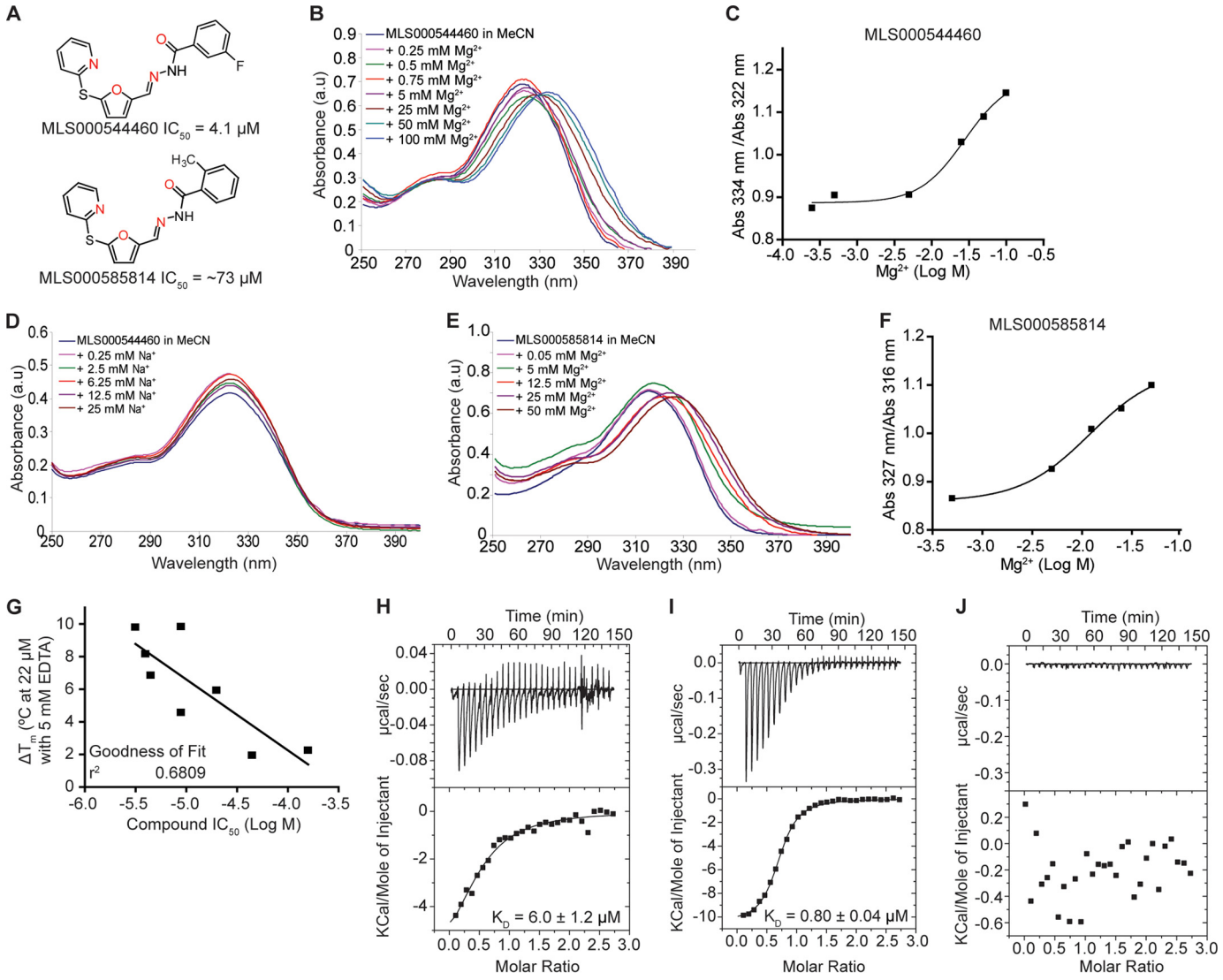

FIGURE 4. **The interaction between Eya2 ED and the *N*-arylidenebenzohydrazide-containing compound does not require Mg^{2+}.** *A*, structures of two active compounds with heteroatoms that can potentially coordinate Mg^{2+} shown in *red*. *B*, UV absorption spectrum of compound MLS000544460 in the presence of Mg^{2+}. λ_{max} shifted from 322 nm to 334 nm with increasing concentrations of Mg^{2+}. *C*, the λ_{max} shift observed in *B* is quantified as a function of Mg^{2+} concentration. *D*, the UV absorption spectrum of MLS000544460 in the presence of Na^{+}. λ_{max} remained at 323 nm when titrated with Na^{+}. *E*, UV absorption spectrum of the low activity analog MLS000585814 in the presence of Mg^{2+}. λ_{max} shifted from 316 to 327 nm with increasing Mg^{2+} concentrations. *F*, the λ_{max} shift observed in *E* is quantified as a function of Mg^{2+} concentration. *G*, the T_m increase caused by the binding of compounds in the presence of 5 mM EDTA correlates with their IC_{50} values, suggesting that these compounds stabilize Eya2 ED when Mg^{2+} is removed. *H*, MLS000544460 binds with lower affinity in the presence of 5 mM Mg^{2+} (K_D = 6.0 ± 1.2 μM). *I*, MLS000544460 has higher affinity toward Eya2 ED when Mg^{2+} is removed with 10 mM EDTA (K_D, 0.80 ± 0.04 μM). *J*, the structurally similar but inactive compound NCGC00241224 does not bind Eya2 ED. *Abs*, absorbance; *a.u.*, absorbance units.

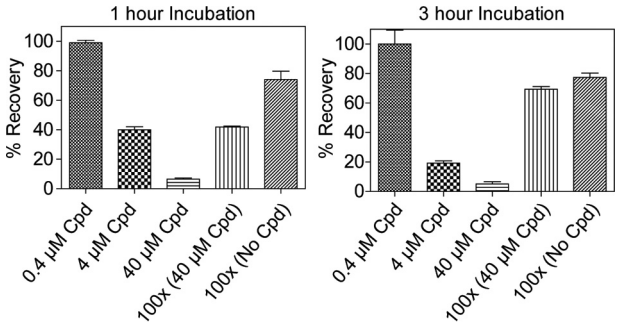

FIGURE 5. **MLS000544460 is a reversible inhibitor.** 1 nM Eya2 ED incubated with various concentrations of MLS000544460 demonstrates that the IC_{50} of MLS000544460 is ~4 μM under this condition (*first three columns* in each panel). The enzymatic activity of Eya2 ED at 1 or 3 h following a 100-fold dilution of 100 nM Eya2 ED incubation with or without MLS000544460 indicate that MLS000544460 is a reversible inhibitor with a slow off rate. *Cpd,* compound.

Identification of Compound-binding Sites Using Crystallography and NMR—Extensive efforts trying to co-crystallize Eya2 ED with MLS000544460 and to soak MLS00544460 into crystals of Eya2 ED (25) were unsuccessful. We next carried out NMR experiments in an attempt to determine the binding site of these compounds. When the active compound MLS000544460 is added to the Eya2 ED at 200 μM concentration, significant changes are observed in the HSQC spectrum of Eya2 ED, including peak shifts and the appearance and disappearance of peaks (Fig. 6). The inactive compound NCGC00241224 does not produce significant changes in the NMR spectrum compared with vehicle control (0.1% DMSO). Unfortunately, the quality of the HSQC spectrum is insufficient (likely due to Eya2 ED aggregates at high concentrations) for us to assign the HSQC spectrum to

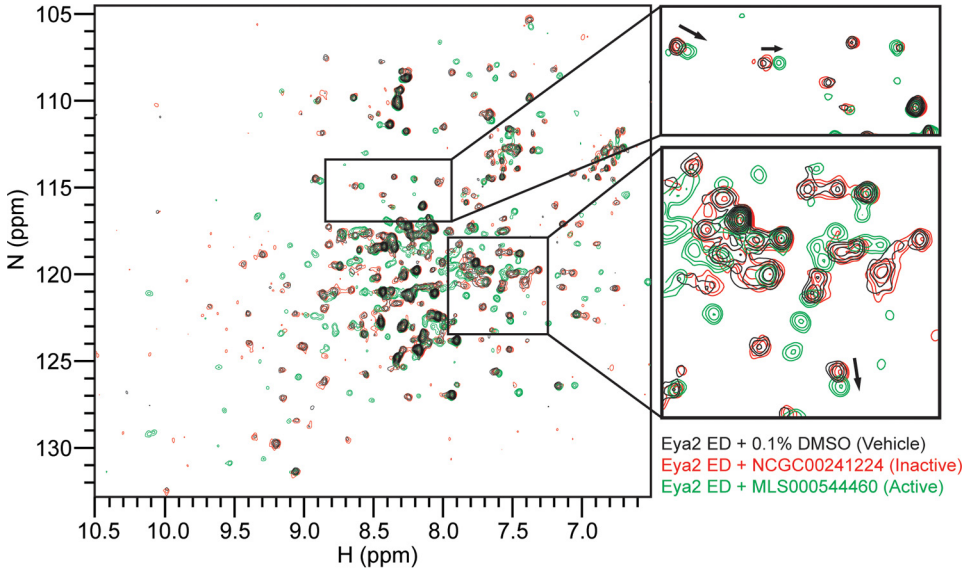

FIGURE 6. **HSQC of ^{15}N-labeled Eya2 ED in the presence of vehicle (DMSO), inactive compound (NCGC00241224), and active compound (MLS000544460).** Select regions are expanded to provide spectrum details. MLS000544460 but not NCGC00241224 generated significant changes in the Eya2 ED HSQC spectrum.

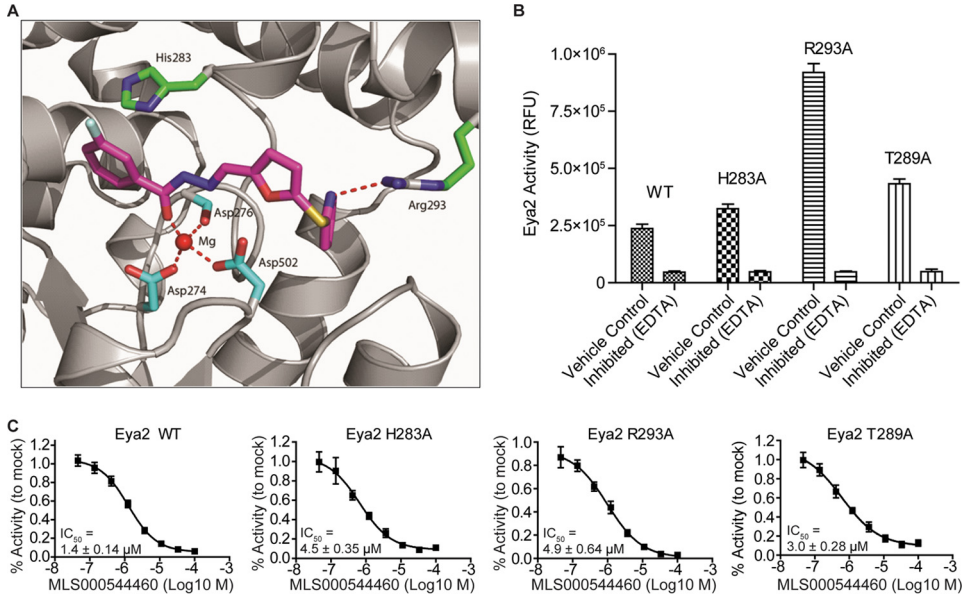

FIGURE 7. **Eya2 inhibitors likely do not bind in the active site.** *A*, a representative docking model of MLS000544460 in the active site. *B*, phosphatase activity of representative active site mutants of Eya2 ED in the presence of DMSO (vehicle control) or EDTA (fully inhibited). *C*, representative dose response curves of active site mutations demonstrate no effect on the ability of MLS000544460 to inhibit the mutant Eya2 ED. The phosphatase activity of Eya2 ED in the presence of DMSO is normalized to 1, and the activity in the presence of EDTA is normalized to 0 in these plots. *RFU,* relative fluorescence units.

identify specific residues in Eya2 ED that interact with the compound.

Mutagenesis Studies Suggest That Compounds Are Not Binding in the Active Site of Eya2—Because crystallography and NMR were unsuccessful in identifying the binding site of these compounds, we used molecular modeling and site-directed mutagenesis to identify potential compound binding sites. As we first embarked on these docking studies, we only had the earlier kinetic data indicating that these compounds are mixed mode inhibitors. In addition, several Eya inhibitors identified by other groups have been proposed to bind in the active site (36) or to a pocket immediately adjacent to the active site (33). We therefore first considered whether our compounds also bind to the active site. Computational docking of molecules of this series in the active site allows their accommodation in several potential binding modes. Fig. 7*A* shows one example of these docking models, where the compound interacts with Mg^{2+}, forming a hydrogen bond with Arg-293 and an aromatic stacking interaction with His-283. To evaluate the validity of these models, we generated mutants that either abolish predicted specific interactions (H283A, T289A, R293A, T448A, T449A, Q450A, E505A, E506A) or sterically block inhibitor binding (T448F and S521F). In addition, three double-mutants (H283A/R293A, T289A/E505A, and T448A/E505A) were generated in case single amino acid mutations were insufficient to affect compound binding. Active site mutants were expressed

and purified in a manner similar to wild type (WT) Eya2 ED and were tested for their phosphatase activity (Fig. 7*B*) as well as their ability to be inhibited by MLS000544460. Of these mutants, E506A and T449A were enzymatically inactive. Some of the remaining mutants displayed decreased activity, but all could still be inhibited by MLS000544460 with similar IC_{50} values (representative dose response curves of several mutants are shown in Fig. 7*C*). These results in combination with our observation that Mg^{2+} is not necessary for the binding of our compounds to Eya2, suggest that the site of interaction for these molecules is not the active site.

```
EYA2_HUMAN SKRSSDPSPAGDNEI|ERVFVWDLDETIIIFHSLLTGTFASRYGKD 297
EYA3_HUMAN GKRKADATSSQDSEL|ERVFLWDLDETIIIFHSLLTGSYAQKYGKD 332
          .**  * :   *.::|****:****************::*.:****

EYA2_HUMAN TTTSVRIGLMMEEMIFNLADTHLFFNDLEDCDQIHVDDVSSDDNGQDLSTYNFSADGFHS 357
EYA3_HUMAN PTVVIGSGLTMEEMIFEVADTHLFFNDLEECDQVHVEDVASDDNGQDLSNYSFSTDGFSG 392
            *  :  ** ******::***********:***:**:**:*********.*.**:*** .

EYA2_HUMAN SAPGANLCLGSGVHGGVDWMRKLAFRYRRVKEMYNTYKNNVGGLIGTPKRETWLQLRAEL 417
EYA3_HUMAN SGGSGSHGSSVGVQGGVDWMRKLAFRYRKVREIYDKHKSNVGGLLSPQRKEALQRLRAEI 452
           *. ...      **:**************:*:*:*:.:*.*****:.  ::*:  :****:

EYA2_HUMAN EALTDLWLTHSLKALNLINSRPNCVNVLVTTTQLIPALAKVLLYGLGSVFPIENIYSATK 477
EYA3_HUMAN EVLTDSWLGTALKSLLLIQSRKNCVNVLITTTQLVPALAKVLLYGLGEIFPIENIYSATK 512
           * *** **  :**:* ** ** ******:*****:************  ***********

EYA2_HUMAN TGKESCFERIMQRFGRKAVYVVIGDGVEEEQGAKKHNMPFWRISCHADLEALRHALELEYL 538
EYA3_HUMAN IGKESCFERIVSRFGKKVTYVVIGDGRDEEIAAKQHNMPFWRITNHGDLVSLHQALELDFL 573
            *********:.***:*..******* :** .**:********: *.** :*::****::*
```

FIGURE 8. **Sequence alignment of Eya2 ED and Eya3 ED.** Residues colored *gray* are not in the ED (which begins at the *bar*) but were in the Eya construct used for phosphatase, ITC, and NMR experiments. *Symbols beneath* sequences represent identical residues (*), strongly similar properties (*colon*), weakly similar properties (*semicolon*), or no similarity (*no symbol*). Residues highlighted in *red* are surface amino acids that were mutated in Fig. 9.

Mutation Analyses Suggest That MLS000544460 Binds in an Allosteric Site—Because the compounds selectively inhibit Eya2 over Eya3, we next examined the amino acid sequence differences between Eya2 and Eya3 as a way to determine where the compound binds. Eya2 ED and Eya3 ED have a 68% sequence identity (Fig. 8). We mapped the amino acid differences to the Eya2 ED crystal structure to identify surface regions that potentially harbor the compound binding sites (Fig. 9*A*). Four sets of mutants were generated that change Eya2 residues to Eya3 on the Eya2 surface (T298P/T300V/S301V/R303G/I304S, T404P/P405Q/W410L/L411Q, L423S/T426G/H427T, and V504R/Q508I) and two additional mutants (Δ359-

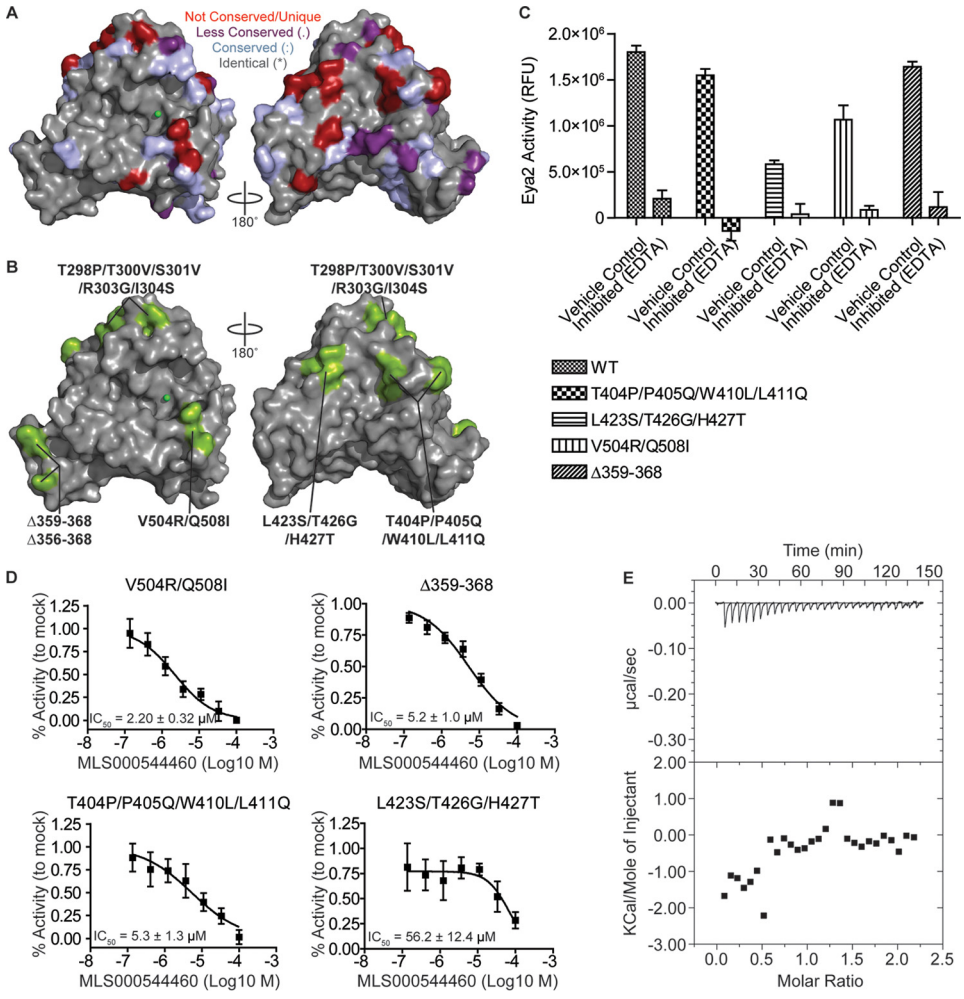

FIGURE 9. **Mutagenesis based on differences between Eya2 and Eya3 ED identifies a potential compound binding site.** *A*, a surface representation of the Eya2 ED structure with surface residues that differ between Eya2 and Eya3 highlighted in different colors. *B*, Eya2 ED mutants generated to change corresponding Eya2 residues to those of Eya3. *C*, phosphatase activity of representative mutants of Eya2 ED in the presence of DMSO (vehicle control) or EDTA (fully inhibited). *D*, dose response curves of Eya2 mutants. One mutant, L423S/T426G/H427T, demonstrated significantly reduced inhibition by MLS000544460, indicating a potential binding site. The phosphatase activity of Eya2 ED in the presence of DMSO is normalized to 1, and the activity in the presence of EDTA is normalized to 0 in these plots. *E*, ITC experiments demonstrate dramatically reduced affinity between the L423S/T426G/H427T and MLS000544460. *RFU,* relative fluorescence units.

368 and Δ356-368) were created that deleted various portions of the unstructured region in the crystal structure that is least homologous between Eya2 and Eya3 ED (Fig. 9*B*). The phosphatase activity of these mutants was tested (Fig. 9*C*), and dose response curves with compound MLS000544460 were generated. All but one set of mutants (L423S/T426G/H427T) were inhibited by MLS000544460 with similar IC_{50} values as the WT. Mutant L423S/T426G/H427T significantly increased the IC_{50} value to 56 ± 12 μM, indicating that compound binding site is greatly affected by the changes of these residues (Fig. 9*D*). ITC experiments confirm that compound MLS000544460 has dramatically reduced binding to the Eya2 ED carrying mutant L423S/T426G/H427T (Fig. 9*E*). These results suggest that the compound is binding near the Leu-423/Thr-426/His-427 region.

We next modeled compound MLS000544460 in the pocket near the L423S/T426G/H427T mutant on the opposite side of the active site (Fig. 10*A*). Energy minimizations of the binding mode indicate that the hydrogen bond interactions involving Glu-418, Thr-426, and Thr-421 at the helix-turn-helix motif between helices 7 and 8 can be disrupted to form a pocket that allows insertion of the pyridine ring of MLS000544460. The compound sits on a largely hydrophobic patch on Eya that involves residues Ile-279, Ile-280, Leu-425, Leu-429, Leu-463, Val-466, and Phe-467. There is also a hydrogen bond interaction between the hydrazone moiety and the main chain of Gly-462. To test this binding model, we designed multiple Eya2 mutants, including L425N, which would be expected to disrupt the hydrophobic surface, and E418W and L417W, which would physically block access to the pocket. These mutants retained enzymatic activity, although at a generally lower activity level than the WT (2–4-fold lower) (Fig. 10*B*). All of these mutants abolished the inhibition of Eya2 ED by MLS000544460 (Fig. 10*C*). ITC experiments using L425N and L417W (Fig. 10*D*) demonstrate no apparent binding, implicating this pocket as the potential allosteric binding site. Mutants R414E and R414A do not have an effect on the inhibition of Eya2 by MLS000544460 (Fig. 10*C*), suggesting that the side chain of Arg-414 is flexible and not directly involved in compound binding. Substitutions of Arg-414 with bulky residues (R414Y and R414W) caused an increase in the IC_{50}, likely through steric interference (Fig. 10*C*).

DISCUSSION

Phosphatases play important roles in multiple disease processes, including cancer, obesity, and type II diabetes (37), yet they have typically been difficult to target, and no phosphatase inhibitors have yet been approved for therapeutic use (38). Difficulty in obtaining small molecules that inhibit phosphatases in a selective manner is a major issue. Because the active sites of phosphatases are generally highly conserved and positively charged, HTS approaches often lead to compounds lacking specificity or that are highly negatively charged, which limits their bioavailability and cell permeability (39).

Eya2 is a member of the unique HAD family of protein Tyr phosphatases that utilize an aspartic acid as the active site residue instead of the cysteine utilized by most cellular phosphatases. We previously exploited this mechanistic difference and carried out a HTS of >330,000 compounds. This screen led to the identification of a series of compounds that demonstrate specificity to Eya2 over other cellular phosphatases, including other HAD family members. This class of compounds displays unexpected high selectivity and does not inhibit or interact with Eya3. This result was surprising as the EDs of Eya2 and Eya3 have 68% sequence identity and 81% similarity, and all of the active site residues are identical or highly conserved. Mutations of residues within the active site of the Eya2 ED revealed no effect on the inhibition of Eya2 phosphatase activity by the compound, suggesting that the compound does not inhibit the phosphatase activity through binding to the active site. This is consistent with the observed compound specificity against Eya2 but not Eya3 as we would expect the compound to inhibit both Eyas if it binds to the active site. The binding between the compound and Eya2 ED also does not require Mg^{2+} (Fig. 4, *G* and *I*). In the absence of Mg^{2+} (with 5 mM EDTA), the increase in binding between Eya2 ED and compounds in the series (reflected by the increase in T_m upon compound binding) correlates with better inhibition (Fig. 4*G*). These observations are all consistent with the notion that the compounds do not bind to the active site and coordinate Mg^{2+}.

We identified a potential binding site for the compound on Eya2 ED that is on the opposite face of the active site, by mutating surface residues differing between the Eya2 and Eya3 ED and evaluating the effect of mutations on the inhibitory activity of the compound. Therefore, our compound likely acts through a novel allosteric mechanism that has not been seen with other HAD inhibitors. Two other groups have identified benzbromarone (33) and metal-chelating compounds (36) as Eya2 phosphatase inhibitors. These Eya inhibitors were proposed to use an Mg^{2+}-chelation mechanism in the active site (36) or to bind in a pocket adjacent to the Mg^{2+} (33). Rabeprazole, the HAD phosphatase inhibitor to Scp1, also binds in a hydrophobic pocket adjacent to the Mg^{2+} in the active site (40). The allosteric mechanism of our compounds is consistent with the kinetic studies under high Mg^{2+} concentrations, which suggest that this series of compounds are non-competitive inhibitors (Fig. 1*B*). At low Mg^{2+} concentrations (*e.g.* 5 μM), these compounds may also inhibit Eya2 phosphatase by chelating Mg^{2+}. Because Eya2 requires Mg^{2+} for enzymatic activity, and because Mg^{2+} is located in the active site, the compound can also act as a competitive inhibitor under low Mg^{2+} conditions. This competition disappears at high concentrations of Mg^{2+}, with the compound acting purely as non-competitive inhibitor.

Although we cannot completely rule out the possibility that mutations around the proposed allosteric site indirectly affect a yet to be identified pocket that is the true compound binding site, multiple lines of evidence suggest that the allosteric site is a direct compound binding site. First, we have made many mutations across the Eya2 ED surface, including the active site, which had no effect on the inhibition of Eya2 ED by our compound, serving as negative controls for our mutagenesis experiments in general. In particular, the T404P/P405Q/W410L/L411Q cluster of mutants contain residues Trp-410 and Leu-411, which are located on the same α7 helix as Arg-414, Leu-417, and Glu-418 whose mutations affect compound inhibition. However, the T404P/P405Q/W410L/L411Q cluster of mutants

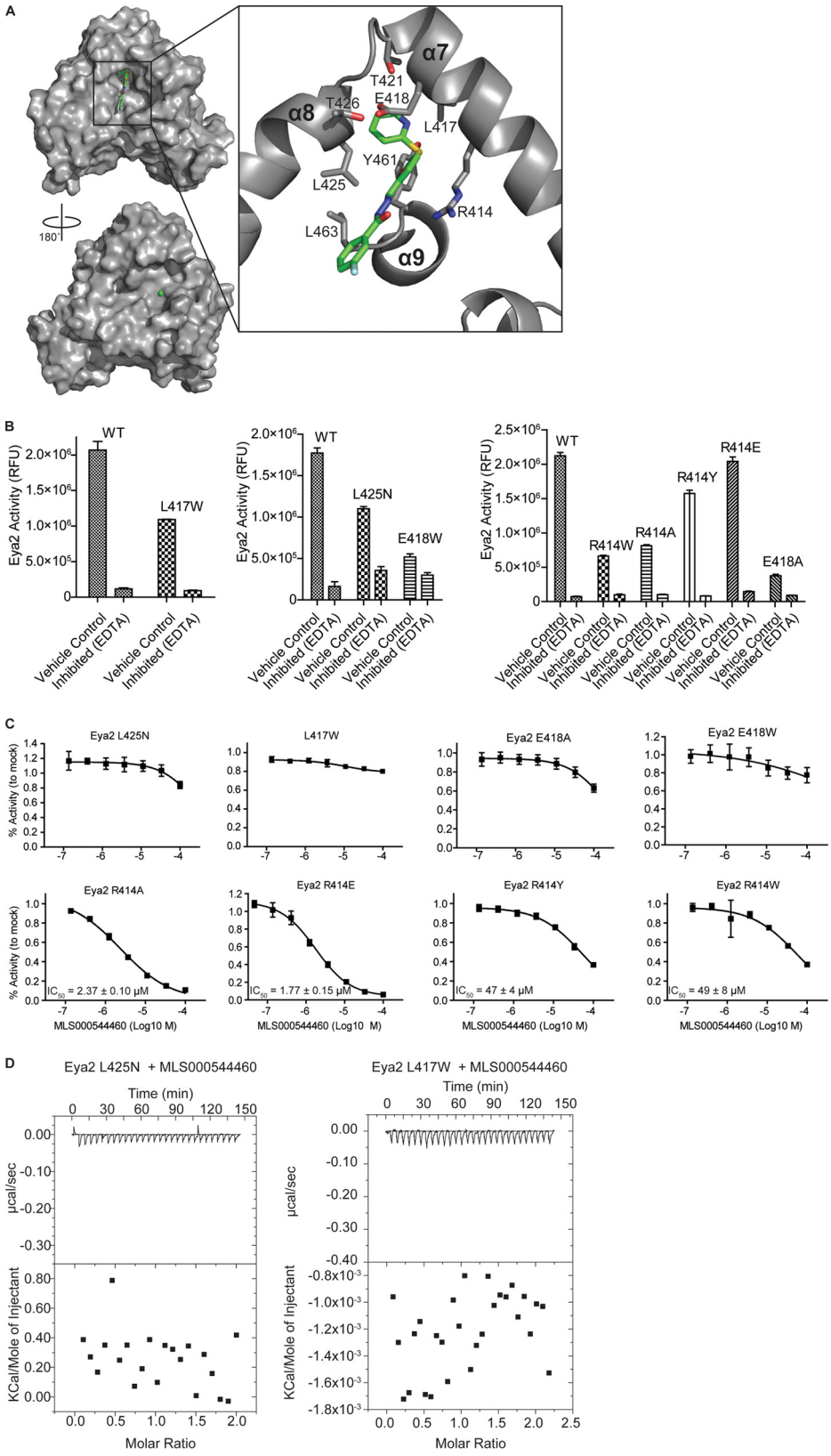

FIGURE 10. **MLS000544460 likely binds to an allosteric site.** *A*, the proposed allosteric compound binding site is on the opposite face of the active site. Compound is shown as a *green* ball-and-stick model, and the Mg^{2+} ion in the active site is represented by a *green sphere*. *B*, a docking model demonstrating residues in the allosteric binding pocket surrounding the compound. *C*, phosphatase activity of representative allosteric site mutants of Eya2 ED in the presence of DMSO (vehicle control) or EDTA (fully inhibited). Various mutants were characterized at different times so they are presented separately with their corresponding WT controls in the same experiment. *D*, effect of mutations in the allosteric binding pocket on the ability of MLS000544460 to inhibit the mutant Eya2 ED. The phosphatase activity of Eya2 ED in the presence of DMSO is normalized to 1, and the activity in the presence of EDTA is normalized to 0 in these plots. *E*, ITC experiments show that MLS000544460 does not bind Eya2 L425N and L417W.

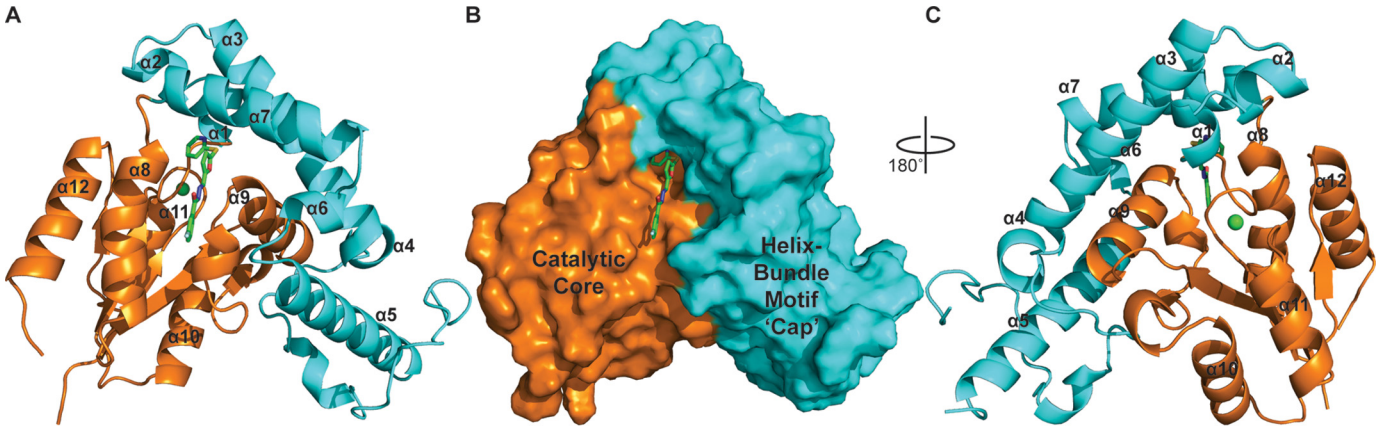

FIGURE 11. **Possible mechanisms of allosteric inhibition by MLS000544460.** *A*, Eya2 is a HAD family member consisting of a catalytic core (*orange*) and a HBM cap (*cyan*). The allosteric compound binding site is located at the interface between these two motifs (α7-α8 loop) (compound is shown in a *green* ball-and-stick model). *B*, surface representation of the catalytic core (*orange*) and HBM (*cyan*) showing MLS000544460 at the interface. *C*, a ribbon diagram demonstrating that the compound (*green*) binds directly behind the catalytic residues centered around the Mg^{2+} ion (*green sphere*). The compound binding at the allosteric site can potentially induce rigidity or conformational changes of the active site pocket.

has no effect on compound inhibition. Second, we have generated four mutations at residue Arg-414. Two of these mutants changed Arg-414 to a dramatically different residue (R414A and R414E) but had no effect on compound inhibition. We only observed interference with compound inhibition when Arg-414 was mutated to bulky residues such as Tyr and Trp. Third, the mutations that do affect compound binding cluster around the binding pocket (instead of scattering all over the Eya2 ED surface) and are located on different secondary structures. It is worth noting that the compounds have a slow off rate and long residence time, as observed by reversibility experiments (Fig. 5), which is highly desirable for a drug and indicates a potential conformational change of the binding site induced by the compound. Our current docking model may not have completely captured the actual binding interaction between the enzyme and the compound after the potential induced fit. We continue to attempt to obtain a co-crystal structure of the compound and Eya2 ED, which would provide the most definitive proof and the most detailed description of the compound-binding mode.

As a member of the HAD family of enzymes, Eya contains a Rossmann-like catalytic core common to all HAD family enzymes (Fig. 11*A*, *orange*) and a unique cap structure consisting of a helix-bundle-motif (HBM) only found in Eya (Fig. 11*A*, *cyan*) (23). Structural homology searches against other HAD enzymes using the DALI server (41) demonstrate that the catalytic core contains a highly conserved structure ($Z = 9.7$–12.3), whereas the HBM cap shows no structural homology with other structures ($Z < 4.0$) (25). Furthermore, a structural homology search of the Eya2 region consisting of the proposed binding site (helix 7, helix 8, and residues forming the base of the pocket (Leu-463, Gly-462, Tyr-461)) displays no homology ($Z < 3.5$) with any other protein structure. The proposed allosteric compound binding site is located at the interface between the catalytic core and the HBM cap (Fig. 11, *A* and *B*). This could provide the selectively against other HAD family of phosphatases, supported by the inactivity of these compounds against Scp1. This proposed binding surface is involved in crystal contacts and is not accessible in the Eya2 ED structures (25), which would explain why we have not been able to obtain compound-containing Eya2 ED crystals in soaking experiments. In the crystal structure of the Six1-Eya2 ED complex (21), the proposed allosteric binding site is solvent-accessible; however, these crystals disintegrate upon soaking with inhibitors, which could be due to conformational changes in Eya2 ED induced by compound binding.

Binding at the interface between the catalytic core and the cap suggests a possible mechanism of inhibition by these compounds. Some HAD members utilize their cap motif for active site solvent occlusion as part of their catalytic mechanism (23). The cap of HAD members is able to move from an "open" conformation where the active site is exposed to a "closed" conformation in which active site access is restricted after substrate binding (23). Because a portion of the active site of Eya2 (on the opposite side of the allosteric compound-binding site) is flanked by helices 1 and 2 of the HBM cap (Fig. 11*C*) and most HAD caps are flexible domains that require movement for catalysis (23), it is possible that these allosteric Eya2 inhibitors lock Eya2 into an open conformation in which active site solvent occlusion cannot occur when substrate binds, consequently inhibiting Eya2 activity. A similar mechanism has been identified for LTV-1, an inhibitor that targets the lymphoid tyrosine phosphatase Lyp, a canonical thiol-based, non-HAD phosphatase involved in T cell antigen receptor signaling. LTV-1 selectively prevents the capping of the "WPD" loop, and the inhibitor can only be modeled into an open conformation of Lyp (42).

Another possibility of how these compounds act as allosteric inhibitors is that these compounds may disturb the active site pocket or induce rigidity in the loops that either contain or are close to residues required for catalysis and coordination of the Mg^{2+} (Asp-274, Asp-276, and Asp-502). Analysis of the crystal structure of Eya2 conjugated to BeF_3 demonstrates that the α4-α5 loop, β2-α9 loop, and β3-α10 loop move laterally compared with the native structure, suggesting intrinsic mobility may be required for catalysis (25). In our model, our inhibitor binds into a pocket directly opposite the active site (Fig. 11*C*). It is possible that the positioning of the compound could either

induce rigidity in the catalytic loops and/or interfere with the geometry of the active site thereby inhibiting catalysis.

The chemical series we identified specifically inhibit Eya2 but not Eya3, although we do not yet know whether these compounds inhibit Eya1 and Eya4 because we have not been able to express and purify human Eya1 and Eya4 from *E. coli*. Multiple amino acids in the allosteric binding pocket of Eya2 whose mutation affected compound inhibition are conserved among all the Eyas (Arg-414, Leu-417, Glu-418, Leu-425) with the exception of Leu-423, Thr-426, and His-427 (Fig. 8). In Eya1 and -4, the Thr-426 residue is conserved but not the Leu-423 and His-427 residues. It is at this point difficult to predict whether this class of compounds will inhibit Eya1 and -4, and further experimental evidence with purified Eya1 and 4 is likely required to address this specificity question.

In summary, we have identified a series of *N*-arylidenebenzohydrazide compounds that specifically inhibits Eya2 but not Eya3 or other cellular phosphatases. These compounds also inhibit Eya2 phosphatase mediated cell migration, suggesting that these compounds could potentially inhibit metastasis. Our previous data suggest that Eya2 is a critical player in breast and ovarian cancers (16, 17). Eya2 is amplified in 14.8% of ovarian cancers (43), where its overexpression is associated with shortened overall survival in advanced ovarian cancer cases (43). In addition, Eya2 cooperates with Six1 to mediate poor prognosis in breast cancers. (Eya1 also shows this cooperation, but not enough breast tumors overexpress Eya3 or Eya4 to enable meaningful analysis of their cooperation with Six1 (17).) Thus, inhibiting the phosphatase of Eya2 is likely to have a significant therapeutic effect in these cancers. We have demonstrated that the *N*-arylidenebenzohydrazide compounds likely bind to an allosteric site on the opposite side of the active site. These molecules are promising lead compounds that can potentially be developed into chemical probes for understanding the function of Eya2 phosphatase or therapeutic agents targeting Eya2 overexpressing tumors.

Acknowledgments—The x-ray and NMR facilities were supported in part by the Structural Biology Shared Resource of the University of Colorado Cancer Center (Grant P30CA046934). We thank Drs. David Jones, Geoffrey Armstrong, Natalie Ahn, and the Ahn laboratory for advice and technical help.

REFERENCES

1. Jemc, J., and Rebay, I. (2007) Identification of transcriptional targets of the dual-function transcription factor/phosphatase eyes absent. *Dev. Biol.* **310,** 416–429
2. Li, X., Oghi, K. A., Zhang, J., Krones, A., Bush, K. T., Glass, C. K., Nigam, S. K., Aggarwal, A. K., Maas, R., Rose, D. W., and Rosenfeld, M. G. (2003) Eya protein phosphatase activity regulates Six1-Dach-Eya transcriptional effects in mammalian organogenesis. *Nature* **426,** 247–254
3. Rayapureddi, J. P., Kattamuri, C., Steinmetz, B. D., Frankfort, B. J., Ostrin, E. J., Mardon, G., and Hegde, R. S. (2003) Eyes absent represents a class of protein tyrosine phosphatases. *Nature* **426,** 295–298
4. Rebay, I., Silver, S. J., and Tootle, T. L. (2005) New vision from Eyes absent: transcription factors as enzymes. *Trends Genet.* **21,** 163–171
5. Grifone, R., Demignon, J., Houbron, C., Souil, E., Niro, C., Seller, M. J., Hamard, G., and Maire, P. (2005) Six1 and Six4 homeoproteins are required for Pax3 and Mrf expression during myogenesis in the mouse embryo. *Development* **132,** 2235–2249
6. Ikeda, K., Ookawara, S., Sato, S., Ando, Z., Kageyama, R., and Kawakami, K. (2007) Six1 is essential for early neurogenesis in the development of olfactory epithelium. *Dev. Biol.* **311,** 53–68
7. Zheng, W., Huang, L., Wei, Z. B., Silvius, D., Tang, B., and Xu, P. X. (2003) The role of Six1 in mammalian auditory system development. *Development* **130,** 3989–4000
8. Wang, Y., Klijn, J. G., Zhang, Y., Sieuwerts, A. M., Look, M. P., Yang, F., Talantov, D., Timmermans, M., Meijer-van Gelder, M. E., Yu, J., Jatkoe, T., Berns, E. M., Atkins, D., and Foekens, J. A. (2005) Gene-expression profiles to predict distant metastasis of lymph-node-negative primary breast cancer. *Lancet* **365,** 671–679
9. Abdelhak, S., Kalatzis, V., Heilig, R., Compain, S., Samson, D., Vincent, C., Levi-Acobas, F., Cruaud, C., Le Merrer, M., Mathieu, M., König, R., Vigneron, J., Weissenbach, J., Petit, C., and Weil, D. (1997) Clustering of mutations responsible for branchio-oto-renal (BOR) syndrome in the eyes absent homologous region (eyaHR) of EYA1. *Hum. Mol. Genet.* **6,** 2247–2255
10. Ruf, R. G., Xu, P. X., Silvius, D., Otto, E. A., Beekmann, F., Muerb, U. T., Kumar, S., Neuhaus, T. J., Kemper, M. J., Raymond, R. M., Jr., Brophy, P. D., Berkman, J., Gattas, M., Hyland, V., Ruf, E. M., Schwartz, C., Chang, E. H., Smith, R. J., Stratakis, C. A., Weil, D., Petit, C., and Hildebrandt, F. (2004) SIX1 mutations cause branchio-oto-renal syndrome by disruption of EYA1-SIX1-DNA complexes. *Proc. Natl. Acad. Sci. U.S.A.* **101,** 8090–8095
11. Zhang, Y., Knosp, B. M., Maconochie, M., Friedman, R. A., and Smith, R. J. (2004) A comparative study of Eya1 and Eya4 protein function and its implication in branchio-oto-renal syndrome and DFNA10. *J. Assoc. Res. Otolaryngol.* **5,** 295–304
12. Coletta, R. D., Christensen, K., Reichenberger, K. J., Lamb, J., Micomonaco, D., Huang, L., Wolf, D. M., Müller-Tidow, C., Golub, T. R., Kawakami, K., and Ford, H. L. (2004) The Six1 homeoprotein stimulates tumorigenesis by reactivation of cyclin A1. *Proc. Natl. Acad. Sci. U.S.A.* **101,** 6478–6483
13. Xu, P. X., Zheng, W., Laclef, C., Maire, P., Maas, R. L., Peters, H., and Xu, X. (2002) Eya1 is required for the morphogenesis of mammalian thymus, parathyroid and thyroid. *Development* **129,** 3033–3044
14. Xu, P. X., Adams, J., Peters, H., Brown, M. C., Heaney, S., and Maas, R. (1999) Eya1-deficient mice lack ears and kidneys and show abnormal apoptosis of organ primordia. *Nat. Genet.* **23,** 113–117
15. Li, C. M., Guo, M., Borczuk, A., Powell, C. A., Wei, M., Thaker, H. M., Friedman, R., Klein, U., and Tycko, B. (2002) Gene expression in Wilms' tumor mimics the earliest committed stage in the metanephric mesenchymal-epithelial transition. *Am. J. Pathol.* **160,** 2181–2190
16. Behbakht, K., Qamar, L., Aldridge, C. S., Coletta, R. D., Davidson, S. A., Thorburn, A., and Ford, H. L. (2007) Six1 overexpression in ovarian carcinoma causes resistance to TRAIL-mediated apoptosis and is associated with poor survival. *Cancer Res.* **67,** 3036–3042
17. Farabaugh, S. M., Micalizzi, D. S., Jedlicka, P., Zhao, R., and Ford, H. L. (2012) Eya2 is required to mediate the pro-metastatic functions of Six1 via the induction of TGF-β signaling, epithelial-mesenchymal transition, and cancer stem cell properties. *Oncogene* **31,** 552–562
18. Wang, Q. F., Wu, G., Mi, S., He, F., Wu, J., Dong, J., Luo, R. T., Mattison, R., Kaberlein, J. J., Prabhakar, S., Ji, H., and Thirman, M. J. (2011) MLL fusion proteins preferentially regulate a subset of wild-type MLL target genes in the leukemic genome. *Blood* **117,** 6895–6905
19. Miller, S. J., Lan, Z. D., Hardiman, A., Wu, J., Kordich, J. J., Patmore, D. M., Hegde, R. S., Cripe, T. P., Cancelas, J. A., Collins, M. H., and Ratner, N. (2010) Inhibition of Eyes Absent Homolog 4 expression induces malignant peripheral nerve sheath tumor necrosis. *Oncogene* **29,** 368–379
20. Auvergne, R. M., Sim, F. J., Wang, S., Chandler-Militello, D., Burch, J., Al Fanek, Y., Davis, D., Benraiss, A., Walter, K., Achanta, P., Johnson, M., Quinones-Hinojosa, A., Natesan, S., Ford, H. L., and Goldman, S. A. (2013) Transcriptional differences between normal and glioma-derived glial progenitor cells identify a core set of dysregulated genes. *Cell Rep.* **3,** 2127–2141
21. Patrick, A. N., Cabrera, J. H., Smith, A. L., Chen, X. S., Ford, H. L., and Zhao, R. (2013) Structure-function analyses of the human SIX1-EYA2 complex reveal insights into metastasis and BOR syndrome. *Nat. Struct.*

Mol. Biol. **20,** 447–453
22. Tootle, T. L., Silver, S. J., Davies, E. L., Newman, V., Latek, R. R., Mills, I. A., Selengut, J. D., Parlikar, B. E., and Rebay, I. (2003) The transcription factor Eyes absent is a protein tyrosine phosphatase. *Nature* **426,** 299–302
23. Seifried, A., Schultz, J., and Gohla, A. (2013) Human HAD phosphatases: structure, mechanism, and roles in health and disease. *FEBS J.* **280,** 549–571
24. Krishnan, N., Jeong, D. G., Jung, S. K., Ryu, S. E., Xiao, A., Allis, C. D., Kim, S. J., and Tonks, N. K. (2009) Dephosphorylation of the C-terminal tyrosyl residue of the DNA damage-related histone H2A.X is mediated by the protein phosphatase eyes absent. *J. Biol. Chem.* **284,** 16066–16070
25. Jung, S. K., Jeong, D. G., Chung, S. J., Kim, J. H., Park, B. C., Tonks, N. K., Ryu, S. E., and Kim, S. J. (2010) Crystal structure of ED-Eya2: insight into dual roles as a protein tyrosine phosphatase and a transcription factor. *FASEB J.* **24,** 560–569
26. Pandey, R. N., Rani, R., Yeo, E. J., Spencer, M., Hu, S., Lang, R. A., and Hegde, R. S. (2010) The Eyes Absent phosphatase-transactivator proteins promote proliferation, transformation, migration, and invasion of tumor cells. *Oncogene* **29,** 3715–3722
27. Wu, K., Li, Z., Cai, S., Tian, L., Chen, K., Wang, J., Hu, J., Sun, Y., Li, X., Ertel, A., and Pestell, R. G. (2013) EYA1 phosphatase function is essential to drive breast cancer cell proliferation through cyclin D1. *Cancer Res.* **73,** 4488–4499
28. Cook, P. J., Ju, B. G., Telese, F., Wang, X., Glass, C. K., and Rosenfeld, M. G. (2009) Tyrosine dephosphorylation of H2AX modulates apoptosis and survival decisions. *Nature* **458,** 591–596
29. Zimmerman, J. E., Bui, Q. T., Steingrímsson, E., Nagle, D. L., Fu, W., Genin, A., Spinner, N. B., Copeland, N. G., Jenkins, N. A., Bucan, M., and Bonini, N. M. (1997) Cloning and characterization of two vertebrate homologs of the *Drosophila* eyes absent gene. *Genome Res.* **7,** 128–141
30. Krueger, A. B., Dehdashti, S. J., Southall, N., Marugan, J. J., Ferrer, M., Li, X., Ford, H. L., Zheng, W., and Zhao, R. (2013) Identification of a selective small-molecule inhibitor series targeting the eyes absent 2 (Eya2) phosphatase activity. *J. Biomol. Screen* **18,** 85–96
31. Koska, J., Spassov, V. Z., Maynard, A. J., Yan, L., Austin, N., Flook, P. K., and Venkatachalam, C. M. (2008) Fully automated molecular mechanics based induced fit protein-ligand docking method. *J. Chem. Inf. Model* **48,** 1965–1973
32. Feig, M., and Brooks, C. L., 3rd. (2004) Recent advances in the development and application of implicit solvent models in biomolecule simulations. *Curr. Opin. Struct. Biol.* **14,** 217–224
33. Tadjuidje, E., Wang, T. S., Pandey, R. N., Sumanas, S., Lang, R. A., and Hegde, R. S. (2012) The EYA tyrosine phosphatase activity is pro-angiogenic and is inhibited by benzbromarone. *PLoS One* **7,** e34806
34. Hojo, M., Ueda, T., and Inoue, A. (2002) UV-visible and ^{1}H NMR spectroscopic studies on direct chelate formation between alkaline earth metal ions and 1-(2-pyridylazo)-2-naphthol or 2-(5-bromo-2-pyridylazo)-5-diethylaminophenol in acetonitrile. *Bull. Chem. Soc. Jpn.* **75,** 2629–2636
35. Kanaya, S., Oobatake, M., and Liu, Y. (1996) Thermal stability of *Escherichia coli* ribonuclease HI and its active site mutants in the presence and absence of the Mg^{2+} ion: proposal of a novel catalytic role for Glu48. *J. Biol. Chem.* **271,** 32729–32736
36. Park, H., Jung, S. K., Yu, K. R., Kim, J. H., Kim, Y. S., Ko, J. H., Park, B. C., and Kim, S. J. (2011) Structure-based virtual screening approach to the discovery of novel inhibitors of eyes absent 2 phosphatase with various metal chelating moieties. *Chem. Biol. Drug Des.* **78,** 642–650
37. Mattila, E., and Ivaska, J. (2011) High-throughput methods in identification of protein tyrosine phosphatase inhibitors and activators. *Anticancer Agents Med. Chem.* **11,** 141–150
38. De Munter, S., Köhn, M., and Bollen, M. (2013) Challenges and opportunities in the development of protein phosphatase-directed therapeutics. *ACS Chem. Biol.* **8,** 36–45
39. Schneider, R., Beumer, C., Simard, J. R., Grütter, C., and Rauh, D. (2013) Selective detection of allosteric phosphatase inhibitors. *J. Am. Chem. Soc.* **135,** 6838–6841
40. Zhang, M., Cho, E. J., Burstein, G., Siegel, D., and Zhang, Y. (2011) Selective inactivation of a human neuronal silencing phosphatase by a small molecule inhibitor. *ACS Chem. Biol.* **6,** 511–519
41. Holm, L., and Sander, C. (1993) Protein structure comparison by alignment of distance matrices. *J. Mol. Biol.* **233,** 123–138
42. Vang, T., Liu, W. H., Delacroix, L., Wu, S., Vasile, S., Dahl, R., Yang, L., Musumeci, L., Francis, D., Landskron, J., Tasken, K., Tremblay, M. L., Lie, B. A., Page, R., Mustelin, T., Rahmouni, S., Rickert, R. C., and Tautz, L. (2012) LYP inhibits T-cell activation when dissociated from CSK. *Nat. Chem. Biol.* **8,** 437–446
43. Zhang, L., Yang, N., Huang, J., Buckanovich, R. J., Liang, S., Barchetti, A., Vezzani, C., O'Brien-Jenkins, A., Wang, J., Ward, M. R., Courreges, M. C., Facchioli, S., Medina, A., Katsaros, D., Weber, B. L., and Coukos, G. (2005) Transcriptional coactivator *Drosophila* eyes absent homologue 2 is up-regulated in epithelial ovarian cancer and promotes tumor growth. *Cancer Res.* **65,** 925–932